atmosphere

MDPI

Article

Multivariate Analysis of Drought Dynamics and Hydroclimatic Variability in San Luis Potosí, México

Maura González Robles [1,2], Jesús López de la Cruz [1,*], Juan Carlos Tejeda González [1] and Teresa Evangelina Martínez Díaz [1]

[1] Faculty of Civil Engineering, University of Colima, Km. 9 Carretera Colima-Coquimatlan, Col. Jardines del Llano, Coquimatlan C.P. 28400, Colima, Mexico; maura.gonzalez@ciad.mx (M.G.R.); tejeda@ucol.mx (J.C.T.G.); teresa_martinez@ucol.mx (T.E.M.D.)
[2] Subsede Colima, Centro de Investigación en Alimentación y Desarrollo (CIAD), SECIHTI, Villa de Álvarez C.P. 28977, Colima, Mexico
* Correspondence: jlopez71@ucol.mx

Abstract

Drought is one of the most complex extreme hydrometeorological phenomena to study and affects extensive regions worldwide. This study aimed to characterize droughts in the state of San Luis Potosí, Mexico. The analysis employed the parametric Standardized Precipitation Index (SPI), based on the two-parameter Gamma distribution. Drought intensity, magnitude, and duration were estimated at a 12-month accumulation time scale (SPI-12) based on records from 194 climatological stations covering the period 1955–2017. Multivariate statistical techniques were applied to identify the main precipitation patterns and the dominant modes of SPI-12 variability. The first two EOF modes explained 67% of the total SPI-12 variance (46% and 21%, respectively), and 14 and 11 drought events were identified for these modes. Significant spatially contrasting associations between the El Niño–Southern Oscillation (ENSO) and drought occurrence and spatial extent were identified. Drought conditions in the Altiplano and Centro regions were more strongly associated with La Niña, whereas the Media and Huasteca regions showed stronger associations with El Niño. Furthermore, the potential utility of SPI-12 as an explanatory covariate for changes in monthly runoff volume records was demonstrated for the Verde and Gallinas river systems, with significant Kendall's tau correlations of 0.330 and 0.380, respectively. The findings provide a basis for improving drought characterization and understanding of its spatiotemporal variability in the region, while offering valuable information to support the development of effective planning, adaptation, and mitigation strategies.

Keywords: hydrological drought; Standardized Precipitation Index (SPI); El Niño-Southern Oscillation; San Luis Potosi

Academic Editors: Muhammad Jehanzaib and Mohammed Achite

Received: 20 July 2026
Revised: 11 October 2026
Accepted: 15 October 2026
Published: 3 November 2026

Copyright: © 2026 by the authors. Licensee MDPI, Basel, Switzerland. This article is an open access article distributed under the terms and conditions of the Creative Commons Attribution (CC BY) license.

1. Introduction

Floods and droughts are among the most significant hydrometeorological hazards worldwide because of their profound economic, environmental, and social impacts [1]. These phenomena clearly demonstrate that, although water is essential for human survival and development, its occurrence in excessive or severely deficient amounts can cause substantial damage. Over recent decades, drought has become a major research topic in hydrology, driven by the need to improve the understanding of its occurrence,

recurrence, behavior, and underlying mechanisms [2–4]. Recent assessments indicate that climate change is intensifying the frequency, duration, and severity of droughts in many regions of the world, particularly in arid and semi-arid environments [5]. Although droughts occur less frequently than floods, hurricanes, and storms [6], they remain among the costliest natural hazards in terms of economic losses and the proportion of affected populations [7]. Their impacts include increased livestock mortality, forest fires, reduced agricultural productivity, declining reservoir storage levels, famine-related diseases, and population displacement [8].

Numerous definitions of drought can be found in the literature. For instance, Linsley [9] defined drought as "a sustained period without significant rainfall," while Schneider [10] described it as "an extended period—a season, a year, or several years of deficient precipitation relative to the long-term statistical mean for a region." Dai [11] characterized drought as "a recurrent extreme climate event over land surfaces, marked by below-normal precipitation over periods ranging from months to years. Likewise, the United Nations Office for Risk Reduction [12] defined drought as "a naturally occurring phenomenon that exists when precipitation has been significantly below recorded normal levels, causing serious hydrological imbalances that adversely affect land-resource production systems." Despite differences in wording, these definitions share two common features: drought is a natural phenomenon, and it originates from persistent precipitation anomalies that may develop in any climatic region, including areas that normally experience abundant rainfall.

An important characteristic of drought is that it can occur under almost any climatic condition. Nevertheless, its manifestations, duration, and impacts vary considerably among regions because they depend on local factors such as precipitation seasonality, temperature, humidity, wind regimes, and physiographic characteristics that influence regional hydroclimatic dynamics. Consequently, drought monitoring and characterization require methodologies capable of capturing both temporal and spatial variability [13]. In this context, standardized drought indices have become essential tools for water resources management and climate risk assessment because of their simplicity, flexibility, and applicability across multiple temporal scales [14].

Mexico is located within a meteorologically complex region influenced by both the Pacific Ocean and the Gulf of Mexico–Caribbean Sea system, in addition to a highly heterogeneous topography. These factors confer distinct hydroclimatic characteristics to each region of the country. Precipitation regimes are strongly controlled by the subtropical high-pressure belt around 30 °N latitude and the Intertropical Convergence Zone (ITCZ) at lower latitudes. Moreover, a wide range of atmospheric and oceanic phenomena modulate climatic variability over Mexico, including the El Niño–Southern Oscillation (ENSO), mesoscale convective systems, tropical cyclones, cold fronts, and the North American Monsoon.

The state of San Luis Potosí represents an especially relevant case study because it lies within a transition zone between the arid and semi-arid environments of northern Mexico and the humid tropical conditions of the Gulf Coastal Plain. This geographic setting generates pronounced climatic and topographic gradients that produce substantial spatial heterogeneity in precipitation regimes and water availability. Furthermore, the state's economy relies heavily on agricultural production and groundwater resources, making it particularly vulnerable to climate variability and drought-related impacts [15]. Despite its importance, relatively few studies have investigated the spatial variability of droughts and their hydroclimatic controls at the state scale.

Several studies have addressed drought occurrence in the region. Among the earliest contributions are regional drought assessments focused on the Media Region using the Foley–Gibbs and Mahé methods [16]. Campos-Aranda [17] proposed a methodology for

constructing drought severity–area–frequency curves and applied it to the San Luis Potosí Valley. Additional studies include comparisons among drought indices based on records from three climatological stations [18] and the application of the Palmer Drought Severity Index to representative locations distributed across the state [19]. However, most previous investigations have concentrated on local analyses or on the comparison of drought indicators, without explicitly addressing the spatial heterogeneity of drought regimes, their links with large-scale climate drivers, or their implications for hydrological systems.

In recent decades, the increasing effects of climate change on precipitation patterns and temperature regimes worldwide have reinforced the need to understand the mechanisms governing drought occurrence and persistence [5]. In particular, identifying the relationships between large-scale modes of climate variability and regional drought dynamics has become a priority for improving drought monitoring and forecasting systems. ENSO is recognized as the dominant source of interannual climate variability worldwide and has been shown to exert a strong influence on precipitation regimes across many regions [20–23]. In Mexico, previous studies have documented significant ENSO-related effects on precipitation variability in states such as Sinaloa, Chihuahua and Baja California [24–26].

Despite the growing body of literature on drought variability in Mexico, important knowledge gaps remain regarding the identification of spatial drought patterns, the regional response to ENSO forcing, and the relationship between meteorological drought and streamflow dynamics. Addressing these issues requires integrated approaches that combine drought indices, multivariate statistical techniques, and hydrological analyses.

The present study contributes to filling these gaps by providing a comprehensive characterization of drought variability in San Luis Potosí through the integration of parametric drought indices, cluster analysis, empirical orthogonal functions, and hydroclimatic analyses. Specifically, the objectives of this study were: (i) to characterize the intensity, magnitude, and duration of drought events using the Standardized Precipitation Index at a 12-month accumulation timescale based on records from 194 climatological stations during the period 1955–2017; (ii) to identify the dominant precipitation regimes across the state; (iii) to determine the principal modes of drought variability using multivariate statistical techniques; (iv) to evaluate the influence of ENSO phases on drought occurrence; and (v) to assess the relationship between drought and surface runoff variability through two representative hydrological systems: the Verde River and Gallinas River basins.

In contrast to previous studies, which have generally focused on individual locations or a limited number of climatological stations, this study uses an extensive network of stations to characterize drought variability across San Luis Potosí at the state scale. Furthermore, the application of empirical orthogonal function analysis provides a spatially explicit identification of the dominant drought patterns and their relationship with ENSO variability, while the integration with streamflow analysis provides an additional perspective on the hydrological expression of drought.

2. Study Area

The state of San Luis Potosí is located in northern Mexico and covers an area of approximately 60,980 km^2, representing 3.3% of the national territory [27]. It is bordered by the states of Zacatecas, Nuevo León, and Tamaulipas to the north; Tamaulipas and Veracruz to the east; Hidalgo, Querétaro, and Guanajuato to the south; and Zacatecas to the west (Figure 1).

For administrative and socioeconomic purposes, San Luis Potosí is divided into four socioeconomic regions: Altiplano, Centro, Media, and Huasteca (Figure 1). According to INEGI [27], the Altiplano Region is the largest, covering 28,236 km^2 and accounting for 46.3% of the state territory. It is followed by the Media Region, which covers 12,605 km^2

(20.6%), the Huasteca Region, with an area of 11,258 km² (18.5%), and the Centro Region, the smallest of the four, covering 8881 km² (14.5%).

From a hydrological perspective, San Luis Potosí lies within two major hydrological regions: the Pánuco Hydrological Region (RH26) and the El Salado Hydrological Region (RH37). The Pánuco Hydrological Region extends over approximately 96,989 km² and recorded a mean annual precipitation of 855 mm during the 1981–2010 climatological period [28]. In contrast, the El Salado Hydrological Region covers an area of 87,801 km² and exhibits a considerably lower mean annual precipitation of 393 mm over the same period [28].

The state presents a marked hydrological contrast, as approximately 45.6% of its territory belongs to RH26, while the remaining 54.4% lies within RH37.

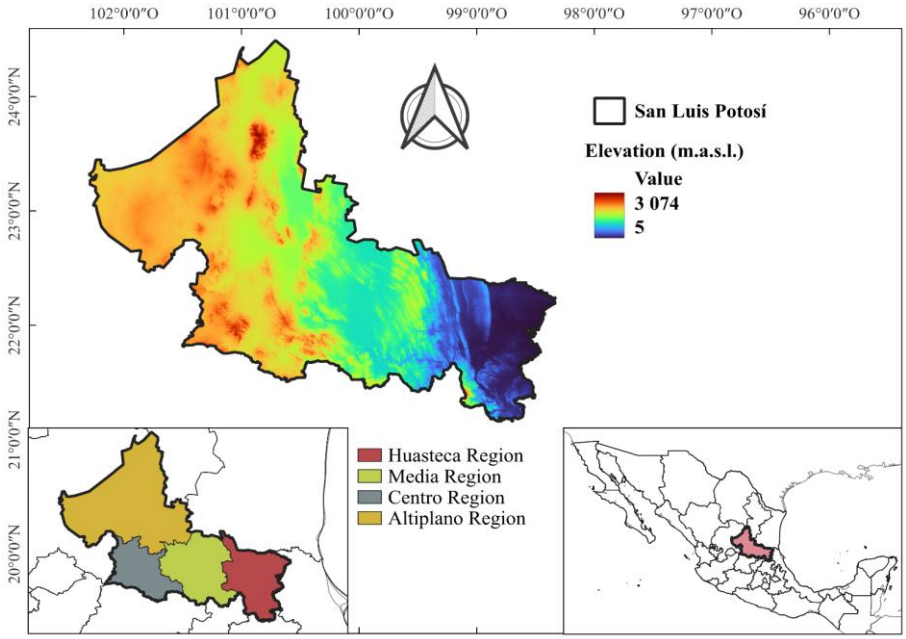


Figure 1. Geographic location of the State of San Luis Potosí, Mexico.

3. Data

Daily precipitation time series, daily mean streamflow records, and the Oceanic Niño Index (ONI) were used in this study. The ONI is based on a threshold of ±0.5 °C, calculated from the three-month running mean of Sea Surface Temperature (SST) anomalies in the Niño 3.4 region. Spatial vector datasets were obtained from the National Water Information System (Sistema Nacional de Información del Agua, SINA; https://sinav30.conagua.gob.mx:8080/SINA/) (accessed on 23 June 2025) and were processed and managed using the open-source Geographic Information System (GIS) software QGIS (version 3.36.0).

3.1. Precipitation Data

Precipitation data were obtained from the database of the Mexican National Meteorological Service (Servicio Meteorológico Nacional, SMN), which provides publicly accessible records that can be downloaded in text-file format. The database is available at: https://smn.conagua.gob.mx/es/climatologia/informacion-climatologica/informacion-estadistica-climatologica, accessed on 21 July 2026. The observations correspond to precipitation accumulated over the preceding 24-h period and are generally recorded at 08:00 a.m. local time [29]. Meteorological stations across Mexico contain varying lengths of historical data, with some records dating back to 1920 and most stations updated through 2018.

Following a preliminary spatial analysis, climatological stations located within and around the state of San Luis Potosí were identified. To account for potential regional

influences near the state boundaries, an initial dataset comprising 287 stations was defined by applying a 20 km buffer zone beyond the state boundaries (Figure 2, left panel). Using the statistical software R (version 4.4.0), station records were analyzed to identify missing data. The study period was established as 1955–2017 based on data availability.

Several quality-control criteria were applied to ensure the reliability of the dataset. Stations with more than 30% missing observations over the study period were excluded from the analysis. In addition, stations with more than 20% missing data during the rainy season (June–October) were also removed. The relatively permissive threshold was adopted to maximize the spatial coverage of the dataset while maintaining an acceptable level of data quality. After applying these selection criteria, the final dataset consisted of 194 climatological stations, whose spatial distribution is shown in Figure 2 (right panel).

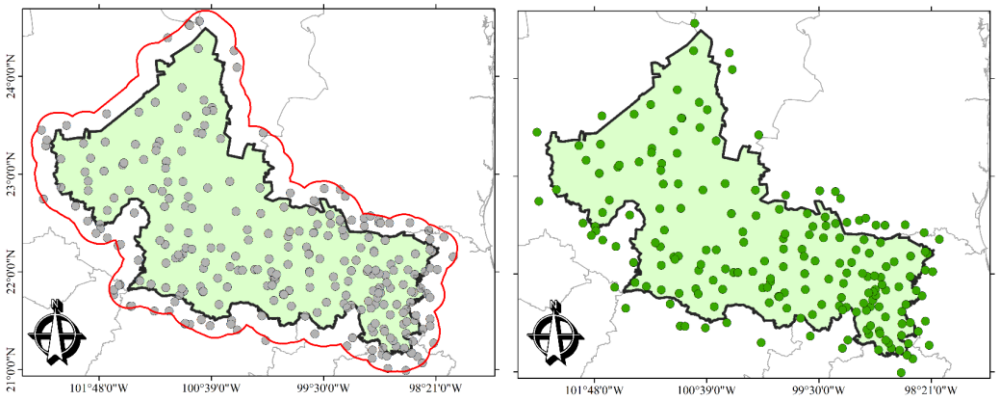


Figure 2. Spatial distribution of the 287 climatological stations comprising the initial dataset (**left panel**) and the 194 stations retained for the analysis after quality-control and data-completeness screening (**right panel**).

3.2. Runoff Data

Monthly runoff volume records were obtained from the National Surface Water Database (Banco Nacional de Aguas Superficiales, BANDAS) maintained by the National Water Commission (CONAGUA). The database is publicly available at: ftp://ftp.conagua.gob.mx/Bandas/Bases_Datos_Bandas. The most recent update available at the time of this study corresponded to 2017.

Table 1 summarizes the main characteristics of the two gauge stations selected for the analysis. Both stations are located within the Media Region of San Luis Potosí and monitor streamflow from two of the state's principal hydrological systems. The Vigas station (26389) is located in the Verde River basin, whereas the Gallinas station (26267) monitors streamflow in the Gallinas River basin.

Table 1. Characteristics of the gauge stations included in the study.

Hydrological Region	Id	Name	Latitude	Longitude	Period of Record
Río Gallinas River	26267	Gallinas	21.9347	−99.2500	1970–2017
Río Verde	26389	Vigas	21.7847	−99.8500	1970–2017

The stations were selected based on the availability of long-term continuous records and their location in basins with natural or minimally altered flow regimes, thereby reducing the potential influence of major anthropogenic disturbances on runoff variability. Given that hydrological drought propagation may be affected by basin storage, groundwater contributions, catchment characteristics, and human interventions, the selected

stations were considered appropriate for assessing the temporal variability of runoff in these two specific basins.

To assess the temporal homogeneity of the streamflow records and identify potential abrupt changes in the flow regime, the non-parametric Pettitt test was applied to the annual runoff volume series derived from the monthly records. A significance level of α = 0.05 was adopted, such that p-values < 0.05 were considered statistically significant. For the Vigas (Verde River) station (26389), the Pettitt test identified 1982 as the candidate change-point year, with a p-value of 0.186. For the Gallinas River station (26267), the candidate change-point year was identified, with a p-value of 0.275 (Table 2). In both cases, the p-values were substantially greater than the adopted significance threshold, indicating that the identified candidate change points were not statistically significant. These results provide evidence of a low degree of detected temporal alteration in the annual runoff records of the two basins during the study period. Consequently, the flow series were considered suitable for characterizing runoff variability and hydrological drought behavior in the Verde and Gallinas basins.

Table 2. Pettitt test results for monthly runoff-volume series.

Station	Pettitt K	Pettitt Break	p Value	Pettitt Result
26267	7317	Nov/1994	0.27527	No significant change point
26389	8554	Mar/1982	0.18651	No significant change point

Both hydrometric stations belong to the Pánuco Hydrological Region (RH26). The drainage area upstream of the Vigas station is 7048.82 km², while the Gallina station drains an area of 940.97 km² (Figure 3). Because of the substantial difference in drainage area and the distinct hydrological characteristics of the two basins, the results and hydrological interpretations presented in this study are restricted to the Verde and Gallinas basins and are not intended to represent the Altiplano, Centro, or Huasteca regions of San Luis Potosí as a whole.

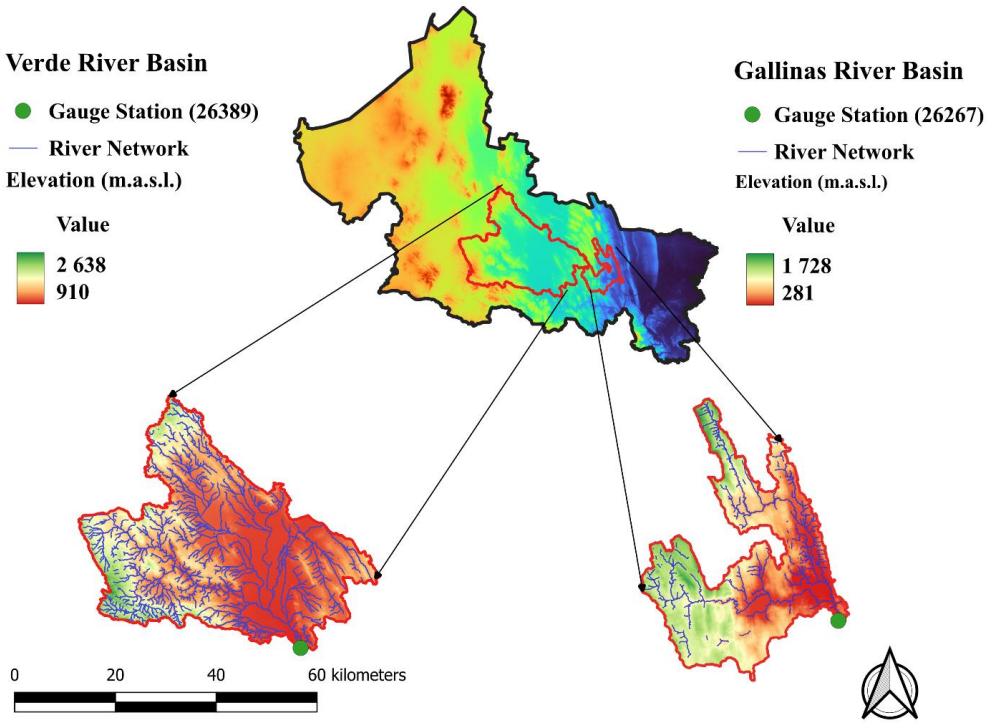


Figure 3. Location of the study basins, showing their elevation ranges and corresponding streamflow gauging stations.

3.3. ENSO Index

This study employs the Oceanic Niño Index (ONI), as defined by the National Oceanic and Atmospheric Administration (NOAA). The corresponding time series was obtained from the NOAA Climate Prediction Center and is publicly available at: https://www.cpc.ncep.noaa.gov/products/analysis_monitoring/enso/oni/v6/, accessed on 21 July 2026.

The ONI is based on sea surface temperature anomalies in the Niño 3.4 region and is used as an indicator of the El Niño–Southern Oscillation (ENSO) to characterize its temporal variability in terms of magnitude and occurrence. This index provides a standardized measure of ENSO. The ONI was adopted in this study to characterize the influence of large-scale climate variability on drought occurrence and hydrological responses in the study area.

4. Methods

4.1. Quality Control and Homogenization of Precipitation Data

Quality control of precipitation time series is a critical step in ensuring the reliability of subsequent analyses. Data homogenization is particularly important because changes in the environment surrounding meteorological stations and/or in observation conditions may introduce artificial discontinuities that affect the consistency of climatic records.

In this study, quality control, missing data infilling, and homogenization were performed using Climatol version 3.1.1 [30], implemented in the R programming environment through RStudio. Climatol reconstructs a reference series for each station using observations from neighboring stations, considering up to ten nearby stations by default and weighting their contributions according to distance. The reconstructed reference series is then compared with the original station record to generate an anomaly series, defined as the differences between the observed and reconstructed values [31]. Unlike methods that assume homogeneous time series a priori, Climatol explicitly accounts for the potential presence of inhomogeneities. The homogenization procedure is based on a relative approach, in which missing values are initially estimated using provisional means and standard deviations [32]. Once the series has been completed, these statistical parameters are recalculated, and the originally missing values are re-estimated. This iterative process continues until successive estimates of the means remain unchanged when rounded to the original data precision.

The homogeneity of the climatic series was evaluated using the Standard Normal Homogeneity Test (SNHT), a widely applied nonparametric procedure for detecting inhomogeneities in climatological records [33]. A comprehensive description of the algorithms and procedures implemented in Climatol is provided in the software user manual [31].

Figure 4 illustrates the temporal availability of daily precipitation records for the 194 climatological stations selected for this study. The analysis showed that 27.32% of the stations had less than 10% missing data, while 62.37% had less than 20% missing data. Only 8.76% of the stations had complete records throughout the entire study period. These results indicate that, although some stations presented missing observations, most of the records had a relatively high degree of completeness and complied with the quality-control criteria established in this study. In particular, the stations included in the analysis were selected considering the predefined thresholds of no more than 30% missing data overall and no more than 20% missing data during the rainy season.

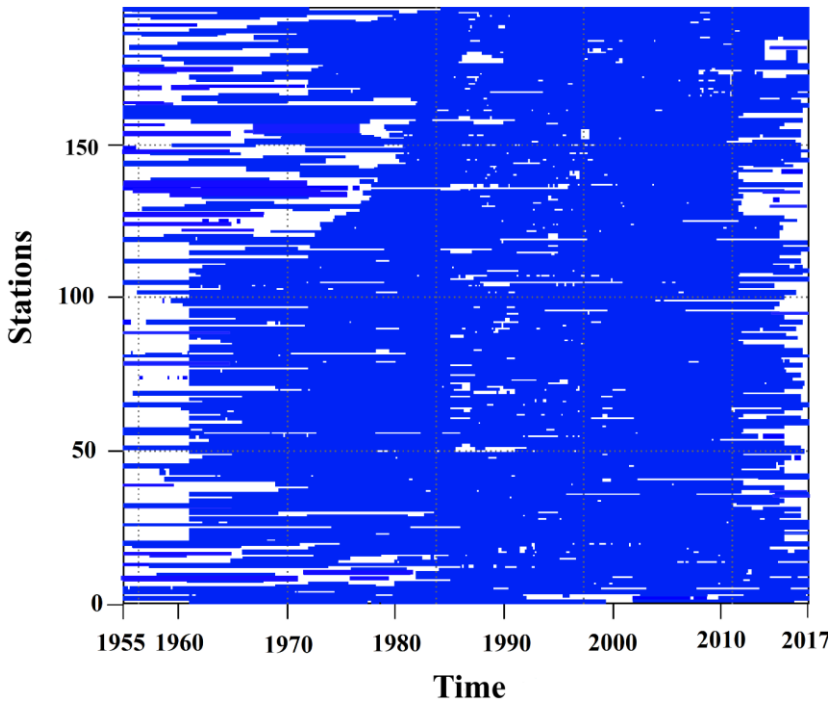


Figure 4. Data availability diagram of daily precipitation records for the 194 climatological stations analyzed using the CLIMATOL package.

Missing observations were reconstructed, and the series homogenized using Climatol. The complete initial network of 287 climatological stations was considered during this procedure, including stations currently classified as suspended, because many of these stations contain valuable historical records, particularly for the 1950–1980 period, and therefore provide additional spatial and temporal information for reconstructing neighboring series. For each missing observation, up to four nearest stations with available data at the corresponding time step were used as references. Climatol estimates missing values using normalized series and weights the contribution of neighboring stations according to geographical distance, thereby allowing records from stations with different climatological means to be combined. After reconstruction and homogenization, the established data-completeness criteria were applied, resulting in a final network of 194 stations used in the subsequent analyses.

The study period was limited to 1955–2017 due to the availability and continuity of climatological records from the National Water Commission (CONAGUA). After 2017, a substantial proportion of the meteorological stations in San Luis Potosí showed discontinuous records, and several stations were subsequently suspended, resulting in increased data gaps and reduced spatial and temporal consistency of the monitoring network. This temporal constraint represents a limitation of the present study, as the results do not capture hydroclimatic variability and drought conditions occurring after 2017.

4.2. Identification of Precipitation Patterns

Spatial patterns of precipitation were identified through hierarchical cluster analysis (HCA), an exploratory multivariate statistical technique widely used to classify observations into homogeneous groups according to their similarity [34]. For the hierarchical cluster analysis, each climatological station was represented by a vector comprising 13 variables: the 12 mean monthly precipitation values corresponding to January through December and the station elevation (m a.s.l.). Prior to the cluster analysis, all variables were normalized to ensure comparability among variables with different measurement scales and to avoid disproportionate influence on the calculation of inter-station distances. These

normalized variables were used to characterize the seasonal precipitation regime and altitudinal conditions of each station. Therefore, the clustering procedure was based on similarities in the mean monthly precipitation patterns and elevation among stations and did not use the complete monthly time series, annual precipitation totals, or monthly anomalies as clustering variables. The analysis was implemented in the R programming environment using the complete linkage agglomeration method, with Euclidean distance adopted as the dissimilarity metric.

Considering a dataset of N precipitation time series described by n variables X_j $(j = 1, 2, \dots \dots, n)$, hierarchical clustering aims to maximize the similarity among series within each cluster while maximizing the dissimilarity between different clusters [34]. This approach facilitates the identification of regions exhibiting similar precipitation regimes and provides an objective basis for the regionalization of precipitation patterns.

4.3. Standardized Precipitation Index (SPI)

The Standardized Precipitation Index (SPI) is a widely used drought indicator that quantifies precipitation deficits over multiple time scales, making it suitable for the assessment of drought conditions of varying duration. Short accumulation periods (e.g., one month) are particularly relevant for agricultural applications, whereas longer time scales are more appropriate for evaluating water availability and hydrological drought [35].

The SPI is computed by fitting the precipitation frequency distribution of the precipitation series X_j $(j = 1, 2, \dots \dots, n)$ to a theoretical probability density function, which is subsequently transformed into a standardized normal distribution [36]. In this study, a two-parameter Gamma probability distribution was adopted to model precipitation data prior to the standardization process.

$$F(x) = \int_0^x \left(\frac{x^{\alpha-1} e^{-\frac{x}{\beta}}}{\beta^{\alpha} \Gamma(\alpha)} \right) dx \tag{1}$$

where α is the shape parameter, β is the scale parameter and $\Gamma(\cdot)$ denotes the Gamma function.

$$\alpha = \frac{1}{4A} \left(1 + \sqrt{1 + \frac{4A}{3}} \right) \tag{2}$$

$$\beta = \frac{\bar{x}}{\alpha} \tag{3}$$

$$A = Ln(\bar{x}) - \frac{\sum_{i=0}^{n} \ln(x)}{n} \tag{4}$$

The cumulative probability distribution is subsequently transformed into a standard normal distribution (with a mean of 0 and a variance of 1), and the resulting standardized values correspond to the Standardized Precipitation Index (SPI) [36]. In this study, the SPI was computed at a 12-month accumulation timescale (SPI-12). This timescale is particularly suitable for identifying long-term meteorological droughts and assessing their impacts on streamflow and water storage conditions, thereby providing an indicator of prolonged hydrological stress.

4.4. Correlation and Variance Analysis

The Kendall's rank correlation coefficient (Kendall's Tau) was used to quantify the degree of association between two variables. As a nonparametric, rank-based statistic, Kendall's Tau is robust to outliers and less sensitive to deviations from linearity than

parametric correlation measures [37]. Similar to other correlation coefficients, Kendall's Tau ranges from −1 to 1, where the sign indicates the direction of the association and the magnitude reflects its strength. Statistical significance was assessed at a 95% confidence level.

To examine the spatiotemporal variability of the Standardized Precipitation Index (SPI), Empirical Orthogonal Function (EOF) analysis was performed. EOF analysis is a widely used variance decomposition technique that identifies the dominant modes of variability in multivariate datasets [38]. In this study, EOF analysis was applied to the SPI-12 dataset to reduce its dimensionality and identify the dominant patterns of temporal variability together with their corresponding spatial distributions. This approach facilitates the interpretation of the principal modes governing long-term drought variability across the study area.

5. Results

5.1. Precipitation Regimes and Temporal Variability

Figure 5 illustrates the spatial distribution of mean monthly precipitation across the state of San Luis Potosí for the 1955–2017 period. A pronounced unimodal precipitation regime is evident, characterized by a well-defined wet season extending from June to October, transitional months in May and November, and a dry season from December to May.

From a spatial perspective, the Huasteca region exhibits the highest precipitation amounts, reflecting the strong influence of moisture transport associated with the dominant atmospheric circulation patterns during the Mexican summer, including tropical cyclones and the northward migration of the Intertropical Convergence Zone (ITCZ). In contrast, the Altiplano and Centro regions represent the driest areas of the state. The Media Region displays an intermediate precipitation regime, with relatively low rainfall in its eastern sector and progressively wetter conditions toward its boundary with the Huasteca region.

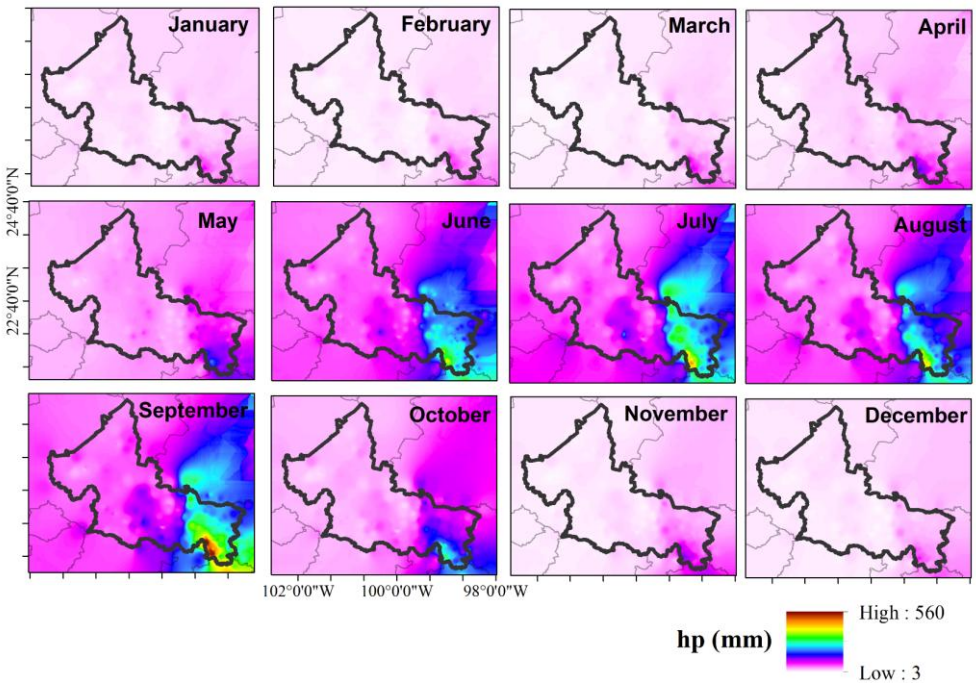


Figure 5. Spatial distribution of mean monthly precipitation across the state of San Luis Potosi.

The results of the hierarchical cluster analysis of precipitation regimes are presented in the dendrogram shown in Figure 6. At a linkage distance of 3000, two major clusters were identified. The first cluster comprises the Media Region and the Huasteca region, whereas the second cluster groups the Altiplano and Centro regions, which exhibit a more

homogeneous precipitation regime. The greater variability observed within the first cluster is readily apparent.

Reducing the linkage distance to 2500 provides a more detailed representation of the clustering structure, revealing three distinct clusters. The first cluster identified at the previous level is subdivided into two groups: the first corresponds to the western sector of the Huasteca region, while the second includes the eastern Huasteca together with the Media Region. The third cluster is composed of the Altiplano and Centro regions.

Based on the hierarchical clustering procedure and the spatial distribution of the resulting groups, a six-cluster solution was adopted to characterize the regional variability of precipitation patterns across the study area.

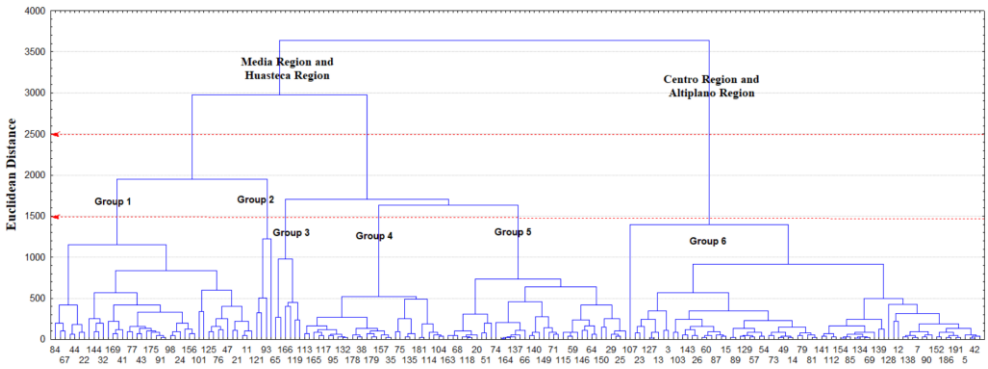


Figure 6. Dendrogram illustrating the hierarchical clustering of precipitation regimes.

Figure 7 shows the spatial distribution of the meteorological stations according to the hierarchical cluster analysis. A high degree of homogeneity in precipitation regimes is evident for the Altiplano and Centro regions, which are grouped within Cluster 6, whereas this cluster exhibits a clear dissimilarity from the Media Region and the Huasteca region.

Most climatological stations within the Media Region are assigned to Cluster 5, indicating relatively homogeneous precipitation characteristics across this region. In contrast, the Huasteca region exhibits the greatest spatial variability, where four homogeneous clusters were identified. Clusters 1 and 2 are primarily located in the central and southern portions of the region, Cluster 3 comprises stations situated along the transition zone between the Media Region and the Huasteca, and Cluster 4 includes the climatological stations located in the northeastern part of the Huasteca region.

The mean monthly precipitation regime for each cluster is presented in Figure 8. All clusters exhibit a well-defined unimodal precipitation regime, although substantial differences are observed in the magnitude of monthly precipitation totals. In five of the six clusters, September corresponds to the month with the highest mean precipitation, indicating the peak of the regional rainy season.

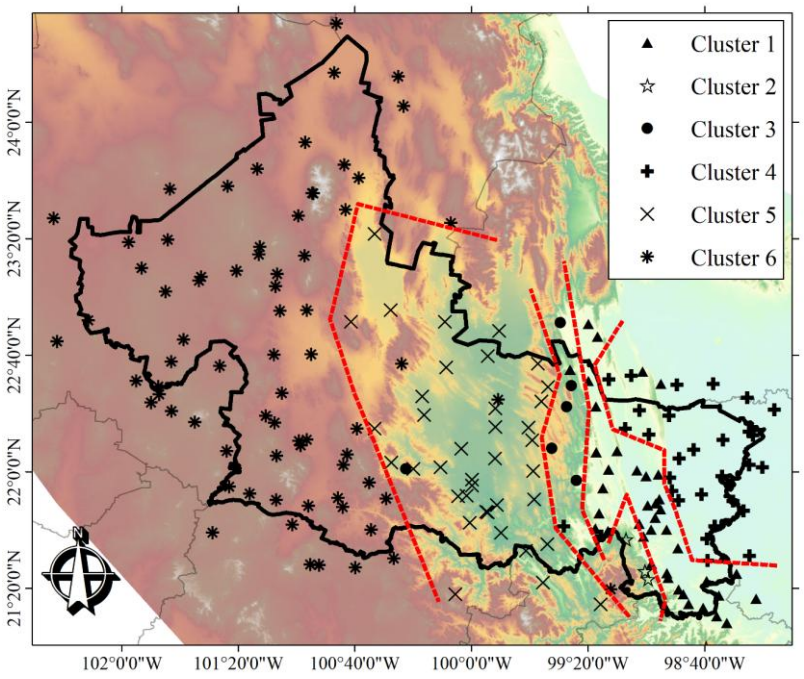


Figure 7. Spatial distribution of the six precipitation regime clusters identified through the multivariate analysis.

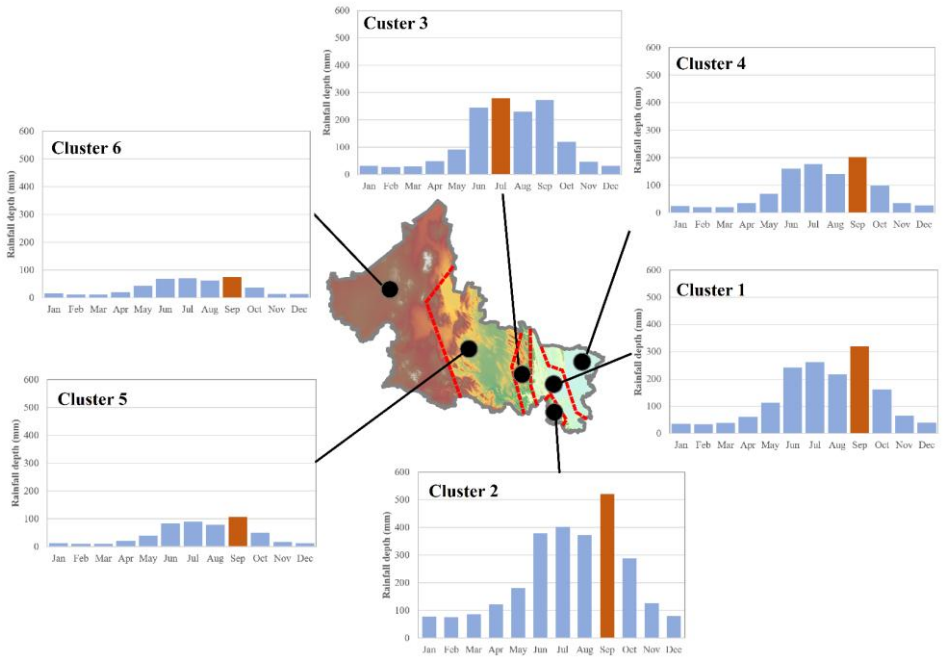


Figure 8. Mean monthly precipitation regimes for the six precipitation clusters.

5.2. Estimation of Drought Magnitude, Duration and Intensity

A Python (version 3.13)-based program was developed to compute the Standardized Precipitation Index (SPI) by implementing the SPI methodology, while data processing and management were performed using the R programming language. The SPI was calculated for each of the 194 climatological stations over the period from January 1955 to December 2017. The analysis was conducted using the 12-month Standardized Precipitation Index (SPI-12), which is suitable for assessing long-term drought conditions and their impacts on water resources.

Positive SPI values indicate precipitation above the long-term mean, whereas negative values indicate below-average precipitation [39]. Because the SPI is a standardized index, both wet and dry conditions can be represented on the same scale, allowing consistent monitoring of hydroclimatic variability over time. Table 3 summarizes the SPI classification and the corresponding drought and wetness categories adopted in the National Drought Monitor of the National Water Commission of Mexico (CONAGUA)

Table 3. SPI classification and corresponding drought and wetness categories.

SPI Value		Condition
≥2		Exceptionally Wet
1.60 to 1.99		Extremely Wet
1.30 to 1.59		Severely Wet
0.80 to 1.29		Moderately Wet
0.51 to 0.79		Mildly Wet
0.50 to −0.50		Near Normal
−0.51 to −0.79		Mildly Dry
−0.80 to −1.29		Moderately Dry
−1.30 to −1.59		Severely Dry
−1.60 to −1.99		Extremely Dry
≤−2		Exceptionally Dry

Once the Standardized Precipitation Index (SPI) had been computed for the 194 climatological stations, Empirical Orthogonal Function (EOF) analysis was performed in RStudio (version 2024.09.1) to examine the dominant modes of spatiotemporal variability. Because the SPI is a standardized index, no additional normalization of the time series was required prior to the analysis.

The results of the EOF analysis are summarized in Figure 9a. The first two EOF modes accounted for 67% of the total variance and were therefore considered representative of the dominant patterns of SPI variability. The first EOF mode explained 46% of the total variance and primarily characterized SPI variability across the Media region and the Huasteca region (Figure 9b). The second EOF mode, which explained 21% of the total variance, was mainly associated with the Altiplano and Centro regions (Figure 9b). Higher-order EOF modes were not considered because the proportion of explained variance decreased markedly beyond the second mode, indicating a limited contribution to the representation of the dominant spatial variability.

The principal drought events identified from the first two EOF modes of the SPI are presented in Figure 10. Drought events were defined as periods during which the SPI remained below −0.50 for at least nine consecutive months, corresponding to mildly dry conditions according to the adopted SPI classification. Based on this criterion, 14 drought events were identified for the first EOF mode and 11 events for the second mode. Several drought episodes affected the entire state, although their timing, duration, and intensity varied among regions. A notable example is the 2011 drought, which exhibited different temporal evolution and severity across the study area.

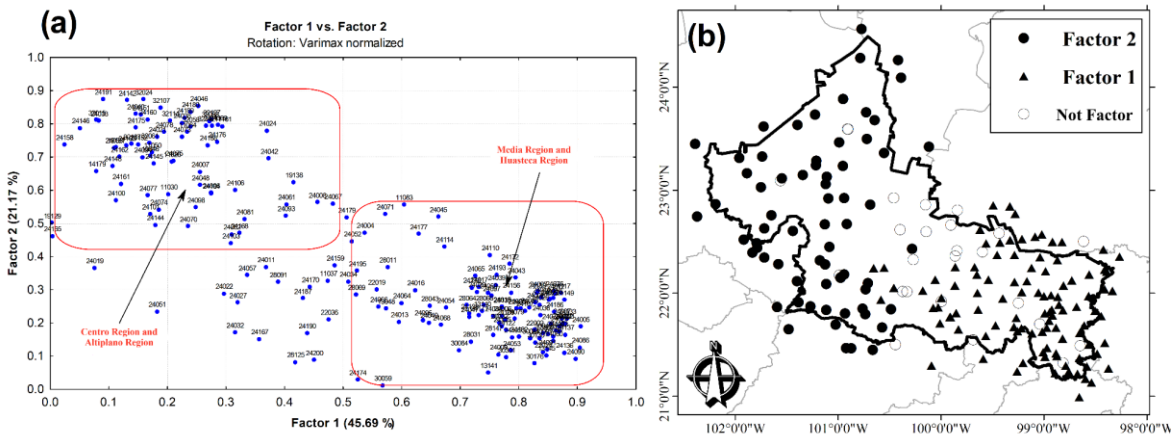


Figure 9. (**a**) Loadings of the first two Empirical Orthogonal Function (EOF) modes extracted from the SPI variance decomposition. (**b**) Spatial distribution of climatological stations with loadings greater than 0.50 for the first two EOF modes.

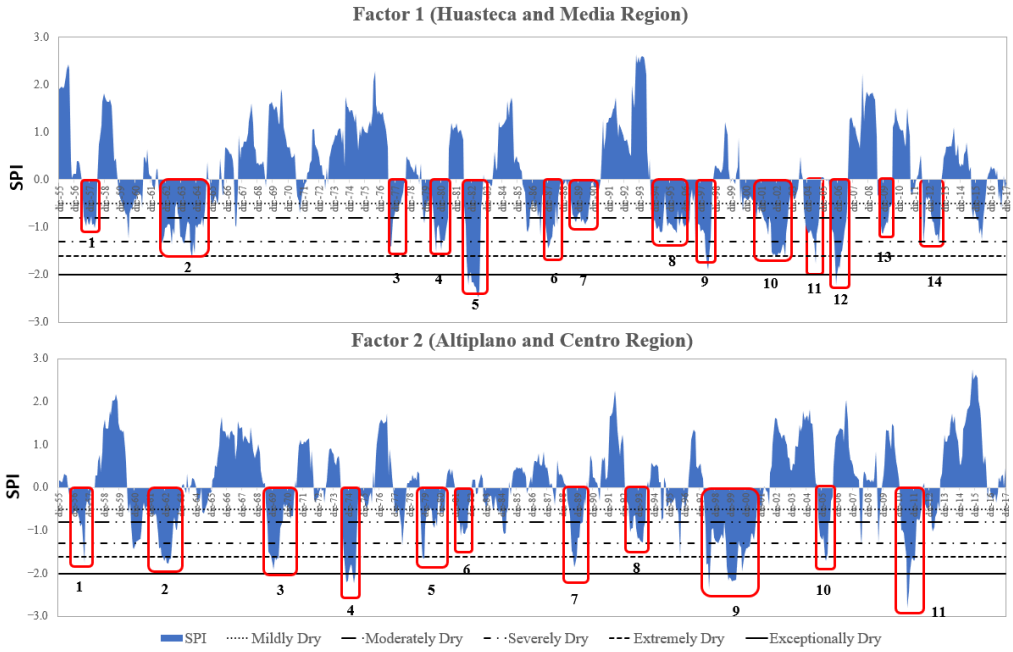


Figure 10. Principal drought events identified from the first two Empirical Orthogonal Function (EOF) modes of the Standardized Precipitation Index (SPI).

Table 4 presents the magnitude, duration, and peak intensity of each identified drought event. The most intense drought associated with the first EOF mode occurred during 1982–1983, whereas the 2011–2012 event exhibited the highest intensity in the second EOF mode. The spatial patterns of these two major drought events are shown in Figures 11 and 12, respectively. The 1982–1983 drought exhibited its greatest severity in the Media and Huasteca regions, whereas the 2011–2012 drought, although affecting most of the state, showed its greatest duration and severity in the Altiplano and Centro regions.

Table 4. Characteristics of the principal drought events identified from the first two Empirical Orthogonal Function (EOF) modes of the Standardized Precipitation Index (SPI).

	No	Magnitude	Peak Intensity	Star Date	End Date	Duration (Months)
Factor1	1	9.71	1.02	jul-57	may-58	11
	2	37.75	1.66	jul-62	jun-65	36
	3	8.22	1.41	jul-77	abr-78	10
	4	13.51	1.51	jun-80	may-81	12
	5	25.93	2.48	jun-82	jul-83	14
	6	11.29	1.44	sep-87	jul-88	11
	7	11.23	0.94	jul-89	aug-90	14
	8	27.86	1.12	sep-94	mar-97	31
	9	17.12	1.89	aug-97	aug-98	13
	10	30.71	1.63	jun-01	sep-03	28
	11	14.03	1.76	sep-04	sep-05	13
	12	18.15	2.22	jul-06	jul-07	13
	13	8.50	1.14	sep-09	jun-10	10
	14	8.20	1.33	jan-13	aug-13	9

	No	Magnitude	Peak Intensity	Star Date	End Date	Duration (Months)
Factor2	1	9.93	1.75	sep-56	sep-57	13
	2	26.97	1.76	dec-61	nov-63	24
	3	1.91	1.91	aug-69	ago-70	13
	4	21.76	2.22	jul-74	jun-75	12
	5	11.46	1.64	sep-79	sep-80	13
	6	8.12	1.11	jan-82	sep-82	9
	7	13.66	1.85	jun-89	abr-90	11
	8	1.28	1.28	may-93	may-94	13
	9	60.53	2.37	abr-98	aug-01	41
	10	11.70	1.71	sep-05	jun-06	10
	11	22.70	2.79	feb-11	may-12	16

The drought events with the greatest magnitude were those occurring during 1962–1965 for the first EOF mode and 1998–2001 for the second EOF mode. The former primarily affected the Media Region and the Huasteca region, whereas the latter predominantly impacted the Altiplano and Centro regions. These events also coincide with the longest drought durations identified in each EOF mode.

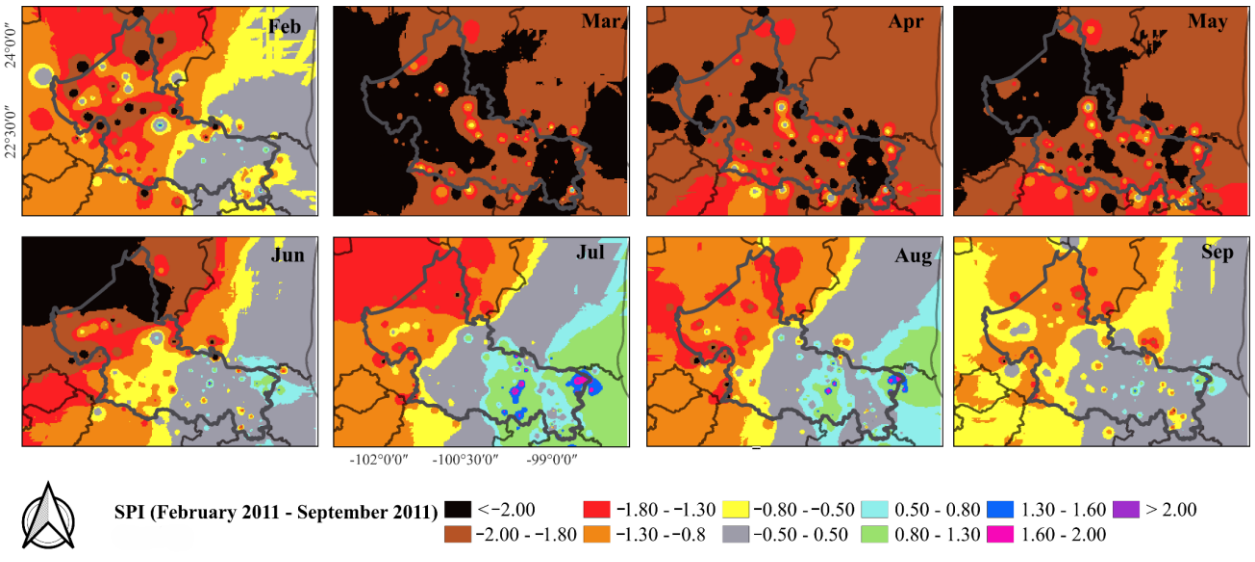


Figure 11. Spatial distribution of the 12-month Standardized Precipitation Index (SPI-12) during 2011.

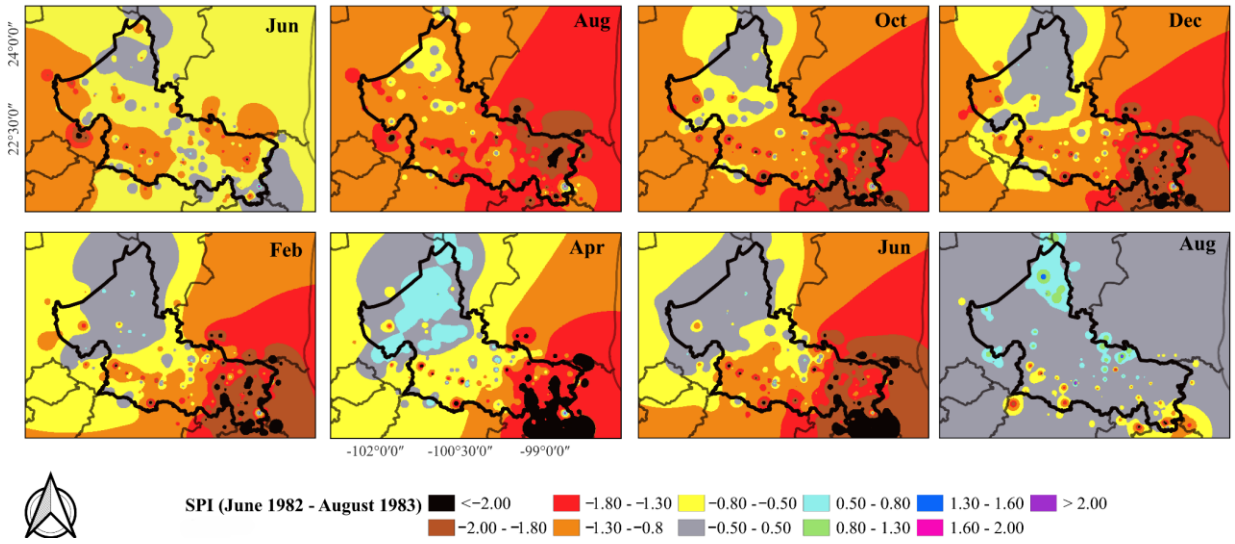


Figure 12. Spatial distribution of the 12-month Standardized Precipitation Index (SPI-12) during 1982–1983.

5.3. Influence of ENSO on the Frequency of Drought Events

The influence of low-frequency climate variability, represented by the El Niño–Southern Oscillation (ENSO), on the occurrence of drought events in San Luis Potosí was evaluated using correlation analysis between the Oceanic Niño Index (ONI) and the dominant modes of SPI variability derived from the Empirical Orthogonal Function (EOF) analysis. The results indicate a statistically significant relationship between ENSO variability and the occurrence of severe drought events.

Figure 13 presents the scatter plots together with the corresponding Kendall's Tau correlation coefficients. Statistically significant correlations were identified at the 5% significance level ($p < 0.05$). Specifically, the first EOF mode of the SPI exhibited a negative correlation with the ONI, whereas the second EOF mode showed a positive correlation with the ONI. These findings suggest that the influence of ENSO on drought variability differs between the dominant precipitation regimes identified in the study area.

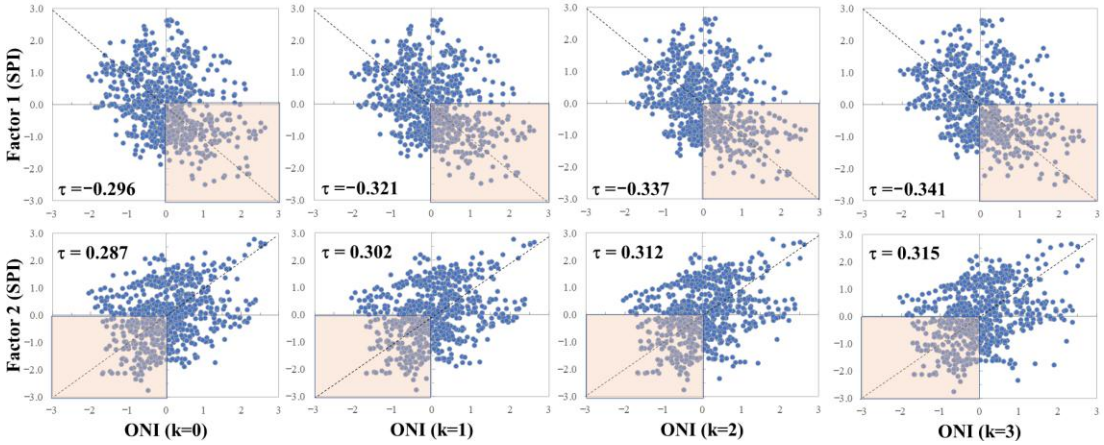


Figure 13. Scatter plots of the two components extracted from the variance analysis of the Standardized Precipitation Index (SPI) and the Oceanic Niño Index (ONI) for different time lags. (k denotes the time lag, in months).

The results indicate that drought events in the Media and Huasteca regions are likely modulated by low-frequency climate variability. The relationship is clearly nonlinear, highlighting the complexity of the underlying climate–drought interactions. The major

droughts that occurred during 1982–1983 and 1997–1998, two of the most severe drought episodes recorded in Mexico, coincided with strong El Niño events (positive ENSO phase). This finding is consistent with previous studies reporting a reduction in precipitation across Mexico during El Niño episodes [40–42].

The occurrence of droughts in the state of San Luis Potosí exhibits a significant relationship with El Niño events, particularly during the most intense episodes (Figure 12). However, the results also indicate that variability in drought frequency across the Altiplano and Centro regions, represented by the second variance component, is more strongly associated with the negative ENSO phase (La Niña). A representative example is the severe drought that affected the state during 2010–2012, with particularly pronounced impacts in the Altiplano and Centro regions. This drought coincided with a strong La Niña event that persisted from June 2010 to March 2012. The highest correlation was observed with a 3-month lag, after which the correlation strength progressively declined.

The relationships identified through the variance analysis are further supported by the correlation surfaces presented in Figure 14. The observed correlations remain relatively stable over time, reflecting the fact that the Oceanic Niño Index (ONI) is derived from sea surface temperature (SST) anomalies, whose temporal evolution is gradual owing to the ocean's large heat storage capacity. Positive correlations are predominantly associated with SPI values calculated at stations located in the Media and Huasteca regions, whereas negative correlations are mainly observed at stations in the Altiplano and Centro regions. Although numerous studies have investigated the influence of ENSO on climate variability in Mexico, the work of Magaña et al. [43] remains one of the earliest and most comprehensive contributions to the subject and continues to serve as a seminal reference in this field.

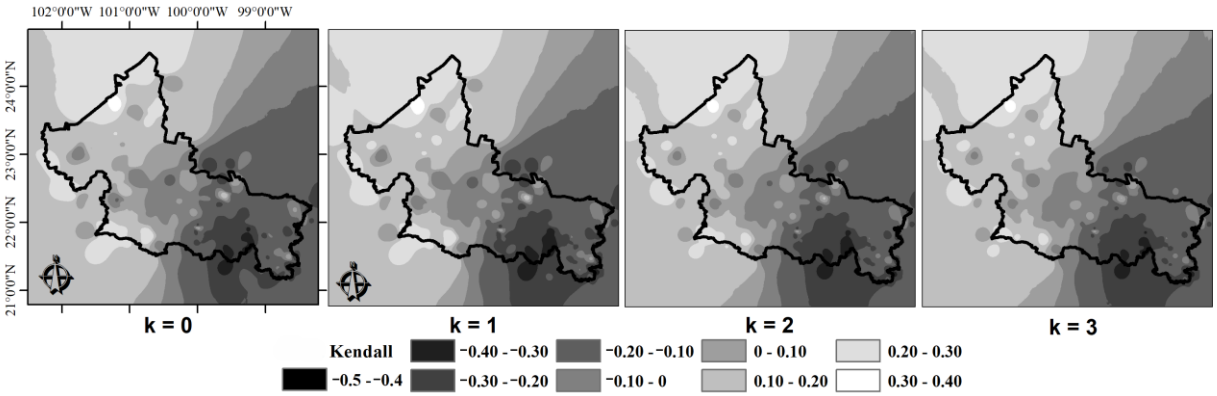


Figure 14. Correlation surfaces between the SPI and ONI. (k denotes the time lag in months).

5.4. Effects of Drought Events on the Variability of Streamflow Regimes in the Verde and Gallinas River Basins

The literature recognizes the Standardized Precipitation Index (SPI), particularly at the 12-month accumulation timescale, as an effective indicator for assessing the impact of precipitation deficits on surface runoff in river systems [44]. This section examines the relationship between the SPI and the variability of streamflow volumes in the Verde River and Gallinas River hydrological systems.

Figure 15 presents scatter plots of the first SPI factor (the first component extracted from the variance analysis) against monthly streamflow volumes, which were computed from the mean daily discharge records obtained from the BANDAS database. The first SPI component was selected because it was found to be statistically associated with precipitation variability in the Media and Huasteca regions. The scatter plots reveal that high streamflow volumes in both basins are associated with positive SPI values, whereas low streamflow volumes correspond to negative SPI values. The Kendall's tau correlation coefficients

were 0.330 for the Vigas hydrometric station and 0.380 for the Gallinas hydrometric station, with both correlations being statistically significant at the 95% confidence level.

An important finding is that streamflow volumes decline markedly once the SPI becomes negative, with the reduction becoming particularly pronounced for SPI values below −0.5. The coherence diagrams shown in Figure 15 indicate that periods of above-normal precipitation allow the hydrological system to recover. However, they also reveal prolonged intervals, lasting several years, during which precipitation remained below the climatological average. Such episodes occurred during 1982–1983, 1997–1998, 2006–2007, and 2010–2011, affecting extensive areas of the state of San Luis Potosí.

The Verde River constitutes the most important hydrological system in the Media region. Based on an analysis of the Public Registry of Water Rights (REPDA), the total water volume allocated within the study basin, upstream of the Vigas hydrometric station, is approximately 197 Mm^3. Groundwater accounts for 74.7% of the allocated water resources, whereas surface water represents only 25.3%. The agricultural sector is the dominant water user, accounting for 86.7% of the allocated volume, followed by the urban public supply sector with 8.0%. As water availability is a key driver of economic development, effective water resources management is essential to ensure long-term water security in the state.

The Standardized Precipitation Index (SPI) represents a valuable tool for the management of surface water resources in San Luis Potosí. Its methodology is straightforward and flexible, enabling its application across multiple accumulation timescales and making it suitable for a wide range of hydrological and water resources management applications.

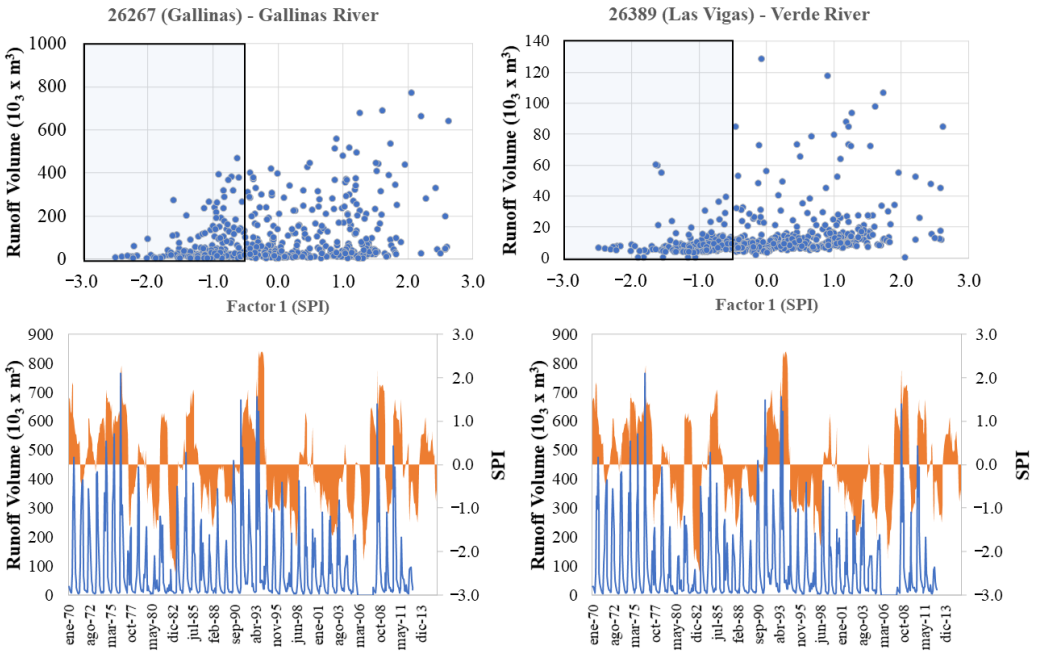


Figure 15. (**Left panel**): association diagrams between SPI and runoff volume in the Verde River basin. (**Right panel**): association diagrams between SPI and runoff volume in the Gallinas River basin.

6. Discussion

The results reveal marked spatial differences in the temporal variability of droughts across the state of San Luis Potosí, reflecting the influence of regional climatic controls and large-scale atmospheric forcing. The cluster analysis identified six precipitation regimes, confirming the pronounced hydroclimatic heterogeneity of the state and highlighting the transition between the arid and semi-arid conditions of northern Mexico and the humid environments associated with the Gulf of Mexico. Similar spatial contrasts have been documented in previous studies, which emphasize the combined effects of topography,

atmospheric circulation, and ocean–atmosphere interactions on precipitation variability over Mexico [45–47].

The precipitation regime in San Luis Potosí is characterized by a predominantly unimodal seasonal pattern, with the rainy season extending from June to October. September represents the month with the highest precipitation totals across most regions of the state. Cluster analysis of precipitation patterns revealed substantial spatial heterogeneity in the climatological precipitation normal, identifying six distinct precipitation groups. The results indicate that the Altiplano, Centro, and Media regions are strongly influenced by the subtropical high-pressure belt, whereas the Huasteca region is primarily affected by the dominant summer meteorological systems over Mexico, including easterly waves, tropical cyclones, and the Intertropical Convergence Zone (ITCZ) [45,48,49]. These systems enhance atmospheric moisture transport into the region, while the pronounced topographic gradient between the coastal lowlands and the higher elevations further modulates the spatial distribution of precipitation.

The contrasting response of the four regions to ENSO variability can be understood in terms of their distinct atmospheric controls. The Altiplano and Centro regions are strongly influenced by the subtropical high-pressure belt over northern Mexico, which limits moisture transport and promotes subsidence conditions. During La Niña events, the strengthening of the Walker circulation and the westward displacement of convection over the tropical Pacific reinforce subsidence over northern Mexico, reducing precipitation and intensifying drought conditions [43,50,51]. Consequently, these regions exhibit a greater sensitivity to cold ENSO phases.

In contrast, the Media and Huasteca regions are more strongly affected by moisture advection from the Gulf of Mexico and by tropical atmospheric systems, including easterly waves, tropical cyclones, and the northward migration of the Intertropical Convergence Zone (ITCZ). During El Niño episodes, anomalous warming in the equatorial Pacific modifies the Walker circulation and alters the position and intensity of the subtropical jet stream, reducing moisture transport toward eastern Mexico and weakening summer convection [50,52,53]. As a result, drought occurrence in these regions appears to be associated primarily with the warm ENSO phase. The contrasting response of the two dominant drought patterns to ENSO can be interpreted in terms of the different climatological and geographic controls on precipitation across San Luis Potosí. In the eastern and wetter region, precipitation is strongly influenced by moisture transport from the Gulf of Mexico and by the interaction between regional circulation and the subtropical high-pressure systems. During El Niño events, changes in the Walker circulation and associated large-scale atmospheric circulation may enhance subsidence and modify the position and intensity of the subtropical high-pressure belt, thereby weakening or redirecting moisture transport toward eastern San Luis Potosí and favoring drier conditions. In contrast, the northern and climatologically drier region has a different moisture regime and is less dependent on persistent Gulf of Mexico moisture transport. Therefore, the same ENSO-related circulation anomalies may have a weaker or different effect on precipitation in this region. The opposite ENSO responses identified by the EOF analysis thus suggest that drought variability in San Luis Potosí is spatially heterogeneous and results from the interaction between large-scale ocean–atmosphere forcing and regional hydroclimatic characteristics, rather than from a uniform ENSO signal across the state.

The nonlinear relationship identified between ENSO variability and drought occurrence confirms that ENSO is not the sole mechanism controlling hydroclimatic extremes in San Luis Potosí. Although several of the most severe drought episodes coincided with major ENSO events—particularly those of 1982–1983, 1997–1998, and 2015–2016—other drought periods occurred under neutral conditions, suggesting the influence of additional modes of climate variability. Previous studies have highlighted the potential contribution

of the Pacific Decadal Oscillation (PDO), the Atlantic Multidecadal Oscillation (AMO), and land atmosphere feedbacks in modulating drought persistence over Mexico [47,54].

The multivariate analysis of SPI-12 revealed coherent drought patterns affecting multiple regions simultaneously, although with differences in duration and intensity. The first component mainly represents drought variability in the Media and Huasteca regions, whereas the second component captures variability associated with the Altiplano and Centro regions. This spatial organization reflects the existence of two dominant hydroclimatic domains within the state: one controlled primarily by continental and subtropical atmospheric processes and another influenced by tropical moisture sources.

The identified drought episodes are consistent with previous studies conducted in Mexico. For example, the severe drought of 2011–2012, recognized as the most intense event affecting the country in recent decades [28], was clearly detected by both principal components. Likewise, the droughts associated with the strong El Niño episodes of 1982–1983 and 1997–1998 have been documented in previous analyses of precipitation variability across northern and central Mexico [50,55].

The analysis of runoff regimes in the Verde and Gallinas river systems demonstrates that SPI-12 constitutes a valuable indicator for understanding hydrological drought propagation. Significant associations between meteorological drought conditions and reductions in runoff volumes were observed in both basins, although the strength of the relationship varied between watersheds. These differences likely reflect basin-specific characteristics, including drainage area, groundwater contributions, storage capacity, land cover, and antecedent moisture conditions. Similar findings have been reported in other Mexican basins, where hydrological responses to meteorological drought exhibit substantial spatial variability [56,57].

From a water-management perspective, the results underscore the potential utility of drought indicators such as SPI-12 for developing early warning systems and supporting decision-making processes. Given the economic importance of agriculture and livestock production in San Luis Potosí, improved drought monitoring could contribute to optimizing reservoir operations, implementing adaptive irrigation strategies, and reducing the vulnerability of rural communities. Moreover, the identification of region-specific responses to ENSO may enhance seasonal forecasting capabilities and strengthen climate adaptation strategies under future climate-change scenarios.

An important limitation of this study is the temporal extent of the climatological records, which restricts the analysis to the 1955–2017 period. Although this interval provides a sufficiently long record to characterize historical drought variability and its spatial patterns across San Luis Potosí, the discontinuity and suspension of several CONAGUA stations after 2017 prevented the inclusion of more recent years without substantially reducing the spatial coverage and consistency of the monitoring network. Consequently, the results presented here should be interpreted as representative of hydroclimatic and drought conditions during the analyzed period and do not account for events occurring after 2017. Future studies incorporating updated and sufficiently consistent observations, as well as complementary data sources such as satellite and reanalysis products.

7. Conclusions

This study characterized meteorological drought variability in San Luis Potosí using SPI-12 records derived from 194 climatological stations spanning the period 1955–2017. The results confirm the existence of pronounced hydroclimatic heterogeneity across the state, driven by the interaction among atmospheric circulation patterns, topographic gradients, and large-scale climate variability.

Cluster analysis identified six precipitation regimes, highlighting substantial differences in rainfall seasonality and magnitude among the Altiplano, Centro, Media, and

Huasteca regions. The Altiplano and Centro regions exhibit a stronger influence of the subtropical high-pressure belt, whereas the Media and Huasteca regions are more strongly affected by moisture transport from the Gulf of Mexico and by tropical atmospheric systems.

The multivariate analysis of SPI-12 revealed two dominant modes of drought variability, allowing the identification of fourteen drought events associated with the first component and eleven events linked to the second component. Several drought episodes affected the entire state, although their temporal evolution and severity varied considerably among regions.

The analysis of ENSO influence demonstrated that drought occurrence in San Luis Potosí is modulated by large-scale climate variability, although the relationship is nonlinear and spatially heterogeneous. The Altiplano and Centro regions exhibit stronger drought conditions during La Niña episodes, whereas drought occurrence in the Media and Huasteca regions is more closely associated with El Niño conditions. These contrasting responses reflect the distinct atmospheric mechanisms governing precipitation across the state.

The association between SPI-12 and runoff volumes in the Verde and Gallinas river basins confirms the usefulness of drought indices for explaining hydrological variability and evaluating the propagation of meteorological drought into surface-water systems. The results suggest that drought indicators can provide valuable information for reservoir management, agricultural planning, and water-allocation strategies.

Given projections of increasing hydroclimatic variability under climate change, strengthening drought-monitoring and forecasting systems is essential to reduce vulnerability in water-dependent sectors. Future research should explore the combined effects of ENSO, the Pacific Decadal Oscillation, and the Atlantic Multidecadal Oscillation, as well as incorporate climate projections and basin-scale analyses to improve drought prediction and support long-term adaptation strategies in San Luis Potosí.

Previous studies based on long-term climate reconstructions have shown that the ENSO teleconnection is non-stationary and that the PDO and AMO can modulate the strength of ENSO-related climate responses [58]. In particular, the PDO appears to exert a stronger influence on ENSO-related hydroclimatic variability than the AMO, although the magnitude and statistical significance of this modulation vary over time. Positive PDO phases may enhance the dry conditions associated with El Niño, whereas negative PDO phases may reinforce the wet conditions associated with La Niña. However, these effects are not necessarily statistically significant throughout the entire record and may occur only during specific periods.

Author Contributions: All authors made substantial contributions to the preparation of the manuscript, data analysis, and visualization of the results. M.G.R., J.L.d.l.C., J.C.T.G. and T.E.M.D. contributed to the conceptualization of the study. J.L.d.l.C. and J.C.T.G. were responsible for data collection and analysis. The methodology was developed by M.G.R., J.L.d.l.C. and T.E.M.D. M.G.R., J.C.T.G. and T.E.M.D. conducted the analysis of precipitation regimes. J.L.d.l.C., M.G.R., and T.E.M.D. contributed to the calculation and analysis of drought events, their relationship with runoff regimes, and the interpretation of the results. All authors contributed to the discussion and conclusions. All authors have read and agreed to the published version of the manuscript.

Funding: This research was supported by the Ministry of Science, Humanities, Technology and Innovation (SECIHTI) through the project "Identification, Management Strategies, and Sustainability Assessment of Water Supply for Urban and Rural Communities in the State of San Luis Potosí within the Framework of the 2030 Agenda".

Institutional Review Board Statement: Not applicable.

Informed Consent Statement: Not applicable.

Data Availability Statement: The original contributions presented in this study are included in the article. Further inquiries can be directed to the corresponding author.

Acknowledgments: The authors gratefully acknowledge the National Water Commission (CONAGUA) for providing the climatological and hydrometric datasets used in this study. They also acknowledge the University of Colima and the Center for Research in Food and Development (CIAD), CEIBAAS Unit, for providing the institutional environment and facilities that supported the completion of this research.

Conflicts of Interest: The authors declare no conflicts of interest.

References

1. World Meteorological Organization (WMO). *State of the Global Climate 2024*; World Meteorological Organization (WMO): Geneva, Switzerland, 2025.
2. Zhao, C.; Brissette, F.; Chen, J.; Martel, J.L. Frequency change of future extreme summer meteorological and hydrological droughts over North America. *J. Hydrol.* **2020**, *584*, 124316. https://doi.org/10.1016/j.jhydrol.2019.124316.
3. Han, J.; Singh, V.P. A review of widely used drought indices and the challenges of drought assessment under climate change. *Environ. Monit. Assess.* **2023**, *195*, 1438.
4. Mukherjee, S.; Mishra, A.; Trenberth, K.E. Climate Change and Drought: A Perspective on Drought Indices. *Curr. Clim. Change Rep.* **2018**, *4*, 145–163. https://doi.org/10.1007/s40641-018-0098-x.
5. IPCC. *Climate Change 2023: Synthesis Report. Contribution of Working Groups I, II and III to the Sixth Assessment Report of the Intergovernmental Panel on Climate Change*; IPCC: Geneva, Switzerland, 2023.
6. EM-DAT. *The International Disaster Database [Internet]*; EM-DAT: Brussels, Belgium, 2020. Available online: https://public.emdat.be/ (accessed on 16 February 2026).
7. Delforge, D.; Wathelet, V.; Below, R.; Landfredi, S.C.; Tonnelier, M.; Van Loenhout, J.A.F.; Speybroeck, N. EM-DAT: The Emergency Events Database. *Int. J. Disaster Risk Reduct.* **2025**, *124*, 105509.
8. García-Jiménez, F.; Fuentes Mariles, O.; Matías Ramírez, L.G. *Sequías*; Serie de Fascículos. Versión El; CENAPRED: Mexico City, Mexico, 2014; 39p.
9. Linsley, R.K. *Hidrología para ingenieros*; McGraw-Hill: New York, NY, USA, 1977.
10. Schneider, S. *Encyclopedia of Climate and Weather*, 2nd ed.; Oxford University Press: New York, NY, USA, 2011; Volume 1.
11. Dai, A. Drought under global warming: A review. *Wiley Interdiscip. Rev. Clim. Change* **2011**, *2*, 45–65. https://doi.org/10.1002/wcc.81.
12. UNDRR. *2021 Global Assessment Report on Disaster risk Reduction: Special Report on Drought [Internet]*; UNDRR: Geneva, Switzerland, 2021. Available online: https://digitallibrary.un.org/record/3946746?v=pdf (accessed on 10 July 2026).
13. Vicente-Serrano, S.M.; Tomas-Burguera, M.; Beguería, S.; Reig, F.; Latorre, B.; Peña-Gallardo, M.; Luna, M.Y.; Morata, A.; González-Hidalgo, J.C. A high resolution dataset of drought indices for Spain. *Data* **2017**, *2*, 22. https://doi.org/10.3390/data2030022.
14. Burić, D.; Mihajlović, J.; Doderović, M.; Mijanović, I. Comparative analysis of SPI and SPEI drought indices for Montenegro and the impact of teleconnections. *J. Water Clim. Change* **2024**, *15*, 5149–5168. https://doi.org/10.2166/wcc.2024.238.
15. Martinez, S.; Delgado, J.; Escolero, O.; Domínguez, E.; Suarez, M. Socio-economic development in arid zones: The influence of water availability in the San Luis Potosi Basin, Mexico. In *Arid Environmental*; Nova Science Publishers: New York, NY, USA, 2010.
16. Flores, I.; Campos, D. Detección de periodos de sequía en la zona media del estado de San Luis Potosí, con base en registros de precipitación mensual. *Tecnol. Cienc. Agua* **1998**, *13*, 45–56.
17. Campos-Aranda, D.F. Caracterización de sequías meteorológicas mediante curvas de severidad-área-frecuencia, en el valle de San Luis Potosí, México. *Tecnol. Cienc. Agua* **2013**, *4*, 165–186.
18. Campos-Aranda, D. Cuantificación de sequías meteorológicas mensuales: Cotejo de cuatro índices en tres localidades de San Luis Potosí, México. *Tecnol. Cienc. Agua* **2017**, *8*, 159–172.
19. Campos-Aranda, D.F. Contrastes del Índice de Sequías de Palmer Estandarizado (SPDI) en tres ubicaciones climáticas de San Luis Potosí, México. *Tecnol. Cienc. Agua* **2018**, *9*, 246–279.
20. Chandimala, J.; Zubair, L. Predictability of stream flow and rainfall based on ENSO for water resources management in Sri Lanka. *J. Hydrol.* **2007**, *335*, 303–312. https://doi.org/10.1016/j.jhydrol.2006.11.024.
21. Muñoz-Díaz, D.; Rodrigo, F.S. Influence of the El Niño-Southern Oscillation on the probability of dry and wet seasons in Spain. *Clim. Res.* **2005**, *30*, 1–12. Available online: http://www.jstor.org/stable/24869228 (accessed on 21 June 2026).

22. Xing, Z.; Yu, Z.; Wei, J.; Zhang, X.; Ma, M.; Yi, P.; Ju, Q.; Wang, J.; Laux, P.; Kunstmann, H. Lagged influence of ENSO regimes on droughts over the Poyang Lake basin, China. *Atmos. Res.* **2022**, *275*, 106218. https://doi.org/10.1016/j.atmosres.2022.106218.
23. Lv, A.; Fan, L.; Zhang, W. Impact of ENSO Events on Droughts in China. *Atmosphere* **2022**, *13*, 1764. https://doi.org/10.3390/atmos13111764.
24. Llanes Cárdenas, O.; Norzagaray Campos, M.; Muñoz Sevilla, P.; Ruiz Guerrero, R.; González Ocampo, H.; Herrera Moreno, M. Estimating Trends and Return Periods of Daily Extreme Precipitation Associated with Tropical Cyclones in the Core North American Monsoon. *Pol. J. Environ. Stud.* **2016**, *25*, 2283–2292.
25. Llanes Cárdenas, O.; Peinado Guevara, H.; Montiel Montoya, J.; Norzagaray Campos, M.; González Ocampo, H.A.; Campista León, S. Seasonal trend indicators and return periods of meteorological drought in the northern states of Mexico. *Pol. J. Environ. Stud.* **2017**, *26*, 1471–1484.
26. Morales, U.R.; Vásquez, B.C.; González, R.P.; Austria, P.M. Influence of the AMO and its modulation of the ENSO effects on summer precipitation in Mexican coastal regions. *Water Pract. Technol.* **2023**, *18*, 304–319. https://doi.org/10.2166/wpt.2023.015.
27. INEGI. *Conociendo San Luis Potosí*; Instituto Nacional de Estadística y Geografía: Aguascalientes, Mexico, 2013; Volume 1, p. 31.
28. CONAGUA. *Estadísiticas del Agua en México 2018*; CONAGUA: Ciudad de México, Mexico, 2018.
29. SMN. *Base de datos de estaciones climáticas*; Servicio Meteorológico Nacional: Mexico City, Mexico, 2025.
30. Guijarro, J.A. *Homogeneización de series climáticas con Climatol*; State Meteorological Agency: Islas Baleares, Spain, 2018.
31. Guijarro, J.A. *User's Guide to Climatology*; State Meteorological Agency: Islas Baleares, Spain, 2011.
32. Pita-Díaz, O.; Ortega-Gaucin, D. Analysis of anomalies and trends of climate change indices in Zacatecas, Mexico. *Climate* **2020**, *8*, 55. https://doi.org/10.3390/cli8040055.
33. Alexandersson, H. A homogeneity test applied to precipitation data. *Climate* **1986**, *6*, 661–675.
34. Romesburg, C. *Cluster Analysis for Researchers*, 2nd ed.; Lulu Press: Durham, NC, USA, 2004; 291p.
35. Loaiza, W.; Carvajal, Y.; Baquero, O. Índice estandarizado de precipitación (SPI) para la caracterización de sequías meteorológicas en la cuenca del río Dagua-Colombia. *Estud. Geogr.* **2015**, *76*, 557–578. https://doi.org/10.3989/estgeogr.201520.
36. Mckee, T.B.; Doesken, N.J.; Keist, J. Influence of climate variability on seasonal rainfall patterns in south-western DR Congo. In Proceedings of the 8th Conference on Applied Climatology, Anaheim, CA, USA, 17–22 January 1993; pp. 17–184.
37. Hirsch, R.; Hesel, D.; Cohn, T.; Gilroy, E. Statistical treatment of hydrologic data. In *Handbook of Hydrology*; Maidment, D., Ed.; McGraw-Hill: New York, NY, USA, 1992.
38. Von Storch, H. Misues of statistical analysis in climate researh. In *Analysis of Climate Variablity: Applications of Statistical Techniques [Internet]*; Springer: Berlin/Heidelberg, Germany, 1995; pp. 11–26. https://doi.org/10.1007/978-3-662-03744-7_2.
39. AEMET. Vigilancia de la Sequía Meteorológica. 2009. Interpretación del Índice de Precipitación Estandarizado (SPI). Available online: https://www.aemet.es/es/serviciosclimaticos/vigilancia_clima/vigilancia_sequia/ayuda (accessed on 21 march 2026).
40. Acosta, V.; De la Parra, M. *Gestión de riesgo de desastre ENSO en América Latina: México*; CIESAS: Ciudad de México, Mexico; 2003.
41. Higareda, C.E.R.; Montijo, B.S.; Martínez, J.C.; Díaz, J.S.; Sauceda, J.M.C. Regional characterization of ENSO effects on the seasonal rainfall of Sinaloa, Mexico. *Atmosfera* **2025**, *39*, 211–224. https://doi.org/10.20937/ATM.53412.
42. Zermeño Díaz, D.M.; Mendoza, L.G. The influence of ENSO during spring over northwestern Mexico. *Int. J. Climatol.* **2023**, *43*, 6420–6433. https://doi.org/10.1002/joc.8212.
43. Magaña, V.; Pérez, J.; Vázquez, J.L.; Carrisoza, E.; Peréz, J. *Los impactos del El Niño en México*; Centro de Ciencias de la Atmósfera, Universidad Nacional Autónoma de México UNAM), Mexico City, Mexico, 1999; pp. 1–121.
44. WMO. *Standarized Precipitation Index User Guide*; World Meteorological Organization (WMO): Geneva, Switzerland, 2012.
45. Magaña, V.; Vázquez Jorge Pérez, J.L.; Pérez, J. Impact of El Niño on precipitation in Mexico. *Geofísica Int.* **2003**, *42*, 313–330.
46. Cavazos, T.; Turrent, C.; Lettenmaier, D.P. Extreme precipitation trends associated with tropical cyclones in the core of the North American monsoon. *Geophys. Res. Lett.* **2008**, *35*, L21703. https://doi.org/10.1029/2008GL035832.
47. Englehart, P.; Douglas, A. The role of eastern North Pacific tropical storms in the rainfall climatology of western Mexico. *Int. J. Climatol.* **2001**, *21*, 1357–1370.
48. Rincón-Avalos, P.; Khouakhi, A.; Mendoza-Cano, O.; López-De la Cruz, J.; Paredes-Bonilla, K.M. Evaluation of satellite precipitation products over Mexico using Google Earth Engine. *J. Hydroinformatic* **2022**, *24*, 711–729. https://doi.org/10.2166/hydro.2022.122.
49. Méndez González, J.; De Jesús Návar Cháidez, J.; Ontiveros, V.G. Analysis of rainfall trends (1920–2004) in Mexico. *Investig. Geográficas* **2007**, *65*, 38–55. Available online: https://www.scielo.org.mx/pdf/igeo/n65/n65a4.pdf (accessed on 13 July 2026).
50. Méndez, M.; Magaña, V. Regional aspects of prolonged meteorological droughts over Mexico and central America. *J. Clim.* **2010**, *23*, 1175–1188. https://doi.org/10.1175/2009JCLI3080.1.

51. Seager, R.; Ting, M.; Davis, M.; Stahle, D.W. Mexican drought: An observational modeling and tree ring study of variability and climate change. *Atmósfera* **2009**, *22*, 1–31. Available online: https://www.scielo.org.mx/scielo.php?script=sci_arttext&pid=S0187-62362009000100001 (accessed on 9 april 2026).
52. Bravo-Cabrera, J.L.; Azpra-Romero, E.; Zarraluqui-Such, V.; Gay-García, C. Effects of El Niño in Mexico during rainy and dry seasons: An extended treatment. *Atmosfera* **2017**, *30*, 221–232. https://doi.org/10.20937/ATM.2017.30.03.03.
53. Colorado-Ruiz, G.; Cavazos, T.; Salinas, J.A.; De Grau, P.; Ayala, R. Climate change projections from Coupled Model Intercomparison Project phase 5 multi-model weighted ensembles for Mexico, the North American monsoon, and the mid-summer drought region. *Int. J. Climatol.* **2018**, *38*, 5699–5716. https://doi.org/10.1002/joc.5773.
54. Pavia, E.G.; Graef, F.; Reyes, J. PDO-ENSO Effects in the Climate of Mexico. *J. Clim.* **2006**, *19*, 6433–6438. https://doi.org/10.1175/JCLI4045.1.
55. Stahle, D.W.; Cook, E.R.; Burnette, D.J.; Villanueva, J.; Cerano, J.; Burns, J.N.; Griffin, D.; Cook, B.I.; Acuña, R.; Torbenson, M.C.; et al. The Mexican Drought Atlas: Tree-ring reconstructions of the soil moisture balance during the late pre-Hispanic, colonial, and modern eras. *Quat. Sci. Rev.* **2016**, *149*, 34–60.
56. Castillo-Castillo, M.; Ibáñez-Castillo, L.A.; Valdés, J.B.; Arteaga-Ramírez, R.; Vázquez-Peña, M.A. Analysis of meteorological drought in the Fuerte River Basin. Mexico. *Water Technol. Sci.* **2017**, *8*, 35–52.
57. Serrano-Barrios, L.; Vicente-Serrano, S.M.; Flores-Magdaleno, H.; Tijerina-Chávez, L.; Vázquez-Soto, D. Variabilidad espacio-temporal de las sequías en la cuenca pacífico norte de México (1961–2010). *Cuad. Investig. Geogr.* **2016**, *42*, 185–204. https://doi.org/10.18172/cig.2857.
58. Wang, N.; Dee, S.; Hu, J.; Steiger, N.; Thirumalai, K. PDO and AMO Modulation of the ENSO–Asian Summer Monsoon Teleconnection During the Last Millennium. *J. Geophys. Res. Atmos.* **2024**, *129*, e2023JD039638. https://doi.org/10.1029/2023JD039638.

Disclaimer/Publisher's Note: The statements, opinions and data contained in all publications are solely those of the individual author(s) and contributor(s) and not of MDPI and/or the editor(s). MDPI and/or the editor(s) disclaim responsibility for any injury to people or property resulting from any ideas, methods, instructions or products referred to in the content.